Unsteady dynamics and mode transitions in hybrid hydrogen–aluminum detonations

Pikai Zhang[a,b,c], Yong Xu[d], Huangwei Zhang[b,c,*], Zheng Chen[a]

[a]SKLTCS, HEDPS, College of Engineering, Peking University, Beijing 100871, China

[b]Department of Mechanical Engineering, National University of Singapore, 9 Engineering Drive 1, Singapore 117576, Republic of Singapore

[c]National University of Singapore (Chongqing) Research Institute, Chongqing 401123, China

[d]Cambridge Centre for Advanced Research and Education in Singapore (CARES), 1 Create Way, CREATE Tower, 138602, Republic of Singapore

Abstract

The hybrid detonation of hydrogen–aluminum mixtures represent a promising fuel combination, leveraging the high energy density of aluminum (Al) and the low ignition energy of hydrogen. This study investigates one-dimensional detonation wave propagation in hydrogen–oxygen–argon mixtures containing suspended Al particles, using a Eulerian–Lagrangian approach. The effects of particle loading and size on detonation dynamics are systematically examined. As the particle loading increases, four distinct regimes of shock propagation behavior are identified, and the transitions among these regimes are interpreted. In particular, two steady propagation modes in Regime I and Regime II are associated with distinct detonation structures: single-front detonation (SFD) and quasi-double-front detonation (quasi-DFD), respectively. For the quasi-DFD structure, a compression region, arising from interphase momentum and heat transfer, forms within the particle induction zone. The destabilization of this compression region is identified as the direct cause of the pulsating phenomenon observed in Regime III. The underlying mechanism of the pulsating detonation wave is analyzed in details. Regime IV is characterized by detonation failure. Besides the gas dynamics, the characteristics of particle-phase combustion are investigated. The results indicate that particle surface reactions transition from being primarily governed by diffusion to being increasingly by surface reaction kinetics, which serves as the fundamental trigger for the onset of unstable detonation. These findings provide valuable insights into the underlying mechanisms of hybrid hydrogen–aluminum detonations.

Keywords: Hybrid detonation; aluminum particle; pulsating shock; particle combustion

[*]Corresponding author e-mail: huangwei.zhang@nus.edu.sg.

Novelty and Significance Statement

This study provides the first comprehensive numerical investigation into the unsteady dynamics and mode transitions of hybrid hydrogen–aluminum (H_2–Al) detonations. While prior research has largely focused on steady-state propagation, this work uniquely reveals the mechanisms underlying pulsating instabilities in hybrid detonations through a coupled Eulerian-Lagrangian framework. By systematically varying Al particle size and loading, four distinct propagation regimes are identified, including a newly observed quasi-double-front detonation structure and its transition to pulsation. The destabilization of the interphase-induced compression zone, and the shift in Al combustion from diffusion-controlled to kinetics-controlled regimes are shown to be critical in triggering instability. These findings provide valuable insights into the understanding of hybrid hydrogen–aluminum detonations.

Author Contributions

P.Z.: conceptualization; methodology; software; validation; data curation; formal analysis; writing—original draft.

Y.X.: formal analysis; investigation and supervision.

H.Z.: conceptualization; formal analysis; writing—review and editing; supervision and project administration.

Z.C.: conceptualization; writing—review and editing; supervision; resources and funding acquisition.

1. Introduction

Multiphase detonation is a high-speed combustion phenomenon characterized by shock-induced reactions occurring within a mixture of gaseous, liquid, or solid components. Its propagation is governed by the intricate coupling between shock waves, chemical reactions, disperse phase dynamics, and phase interactions [1, 2]. Following Veyssiere [3], multiphase detonations can be broadly classified into three categories: (1) dusty detonation, in which the gas phase is combustible while the particulate phase is inert, exemplified by hydrogen-dust detonation [4]; (2) heterogeneous detonation, where the gaseous phase is non-combustible, but the particulate phase is reactive, as observed in aluminum (Al) particle [5] and coal particle [6] detonations; (3) hybrid detonation, in which both gas and particulate phases are combustible, with notable examples including methane-char [7] and hydrogen-aluminum [3] detonations. Notably, solid aluminum possesses exceptional energetic potential, with a specific enthalpy of reaction (83.8 MJ/L) approximately seven times greater than liquid ammonia (11.5 MJ/L) and ten times that of liquid hydrogen (8.5 MJ/L) [8]. However, pure Al-air mixture present significant challenges for detonation initiation due to high ignition temperature and relatively slow reaction kinetics [3]. In contrast, hydrogen (H_2) requires significantly lower ignition energy, making it more conducive to detonation initiation. This synergy makes H_2-Al mixtures an attractive hybrid fuel system for detonation propulsion applications, combining hydrogen's ease of initiation with aluminum's high energy density for enhanced performance.

In hybrid detonations fueled by H_2-Al mixtures, introduction of disperse particles significantly alters the propagating wave structures. For instance, unique double-front detonation (DFD) structure was first experimentally observed by Veyssiere [9] in H_2-Al-air mixtures. The first front originates from the combustion of gas components, while the second front results from Al surface reactions occurring in the gaseous products. Subsequent studies [10-13] have consistently confirmed the existence of such DFD mode. Veyssiere and his co-workers [14] further conduct a study comparing two distinct stable propagation modes in H_2-Al mixture: double-front detonation and single-front detonation (SFD). They fundamentally depend on the temporal or spatial sequence of heat release

behind the shock wave. Specifically, the SFD structure occurs when the Al reaction zone resides within the Chapman-Jouguet (CJ) plane of the gas phase. Recent H_2-Al explosion experiments by Yu et al. [15] revealed that reduced particle size facilitates the transition from double-peak to single-peak flame front, attributed to earlier ignition of finer particles. More recently, Khmel and Lavruk's study [16] demonstrated that introduction of small amount of 3.5 and 5 μm Al particles produces transient double-front structures that evolve into single-front detonation through wave merging. This leads to wave acceleration and increased stability, with the transition occurring more rapidly with smaller particles. In summary, extensive experimental and numerical studies have shown that larger particles preferentially form DFD mode due to longer ignition delays, while smaller particles tend to promote SFD mode.

Despite the extensive studies on hybrid H_2-Al detonations, several critical knowledge gaps remain in our understanding of detonation dynamics in H_2-Al mixtures. First, a comprehensive parametric investigation on the effects of particle size and loading on mode transitions and wave structures is still lacking. Second, existing research has predominantly focused on steady-state propagation modes, with limited attention to unsteady dynamics in H_2-Al hybrid detonation systems. However, in practical applications, hybrid detonations are inherently unstable. While pulsating phenomena have been observed in some Al-induced detonation studies [12, 17, 18], the underlying mechanisms and characteristics of these instabilities remain largely unexplored. In contrast to hybrid detonation systems, pulsating propagation in gaseous detonations (e.g., hydrogen-air) has been extensively studied [19-22], where the fundamental mechanisms are relatively well understood. However, similar studies in hybrid detonation systems are scarce, leaving a significant gap in the fundamental mechanisms governing hybrid detonation stability and transition dynamics. This hinders the development of effective control strategies for hybrid detonation-based propulsion systems and limits our ability to predict their performance accurately.

Based on the above analysis, this study aims to investigate the dynamics of hybrid detonation fueled by H_2-Al mixtures through detailed simulations. The purpose of this work is two-fold: (1) to

examine the effects of particle loading and diameter on detonation wave structure and mode transitions, (2) to reveal the underlying physical mechanisms governing pulsating propagation, analyzed from both gas dynamic and particle dynamic perspectives. This enables a comprehensive understanding of the complex interplay between Al particle properties and detonation wave dynamics, providing insights into both macroscopic propagation behaviors and microscopic interaction mechanisms. The manuscript is organized as follows: Sections 2 and 3 introduce the physical model and numerical methods, respectively; Section 4 provides comprehensive results and discussion; and Section 5 summarizes the main conclusions.

2. Physical model

In this study, a one-dimensional (1D) computational configuration is employed to investigate the propagation of hybrid detonation waves in hydrogen-aluminum mixtures. The 1D configuration excludes the transverse wave effects, isolating longitudinal instabilities for ease of analysis. It is widely used in single- and two-phase detonation studies [23, 24] as a standard benchmark for fundamental dynamics with high computational efficiency.

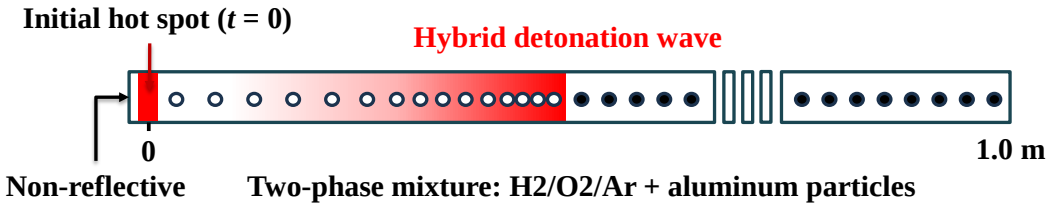

Fig. 1 Schematic of hybrid detonation wave propagation in a $H_2/O_2/Ar$ mixture containing aluminum particles. Solid circles represent aluminum particles, while open circles denote alumina particles.

As illustrated in Fig. 1, the detonation wave is initiated by a hot spot (2,000 K and 20 atm) near the left end of the domain. Changing the hot spot conditions (e.g., higher pressure) may influence early detonation propagation stage, this study focuses on analyzing the long-term detonation wave behavior beyond the transition stage (e.g., $x > 0.3$ m in Fig. 3a). The left boundary is non-reflective for pressure to prevent wave reflections, while zero-gradient for other variables. Similarly, the right boundary utilizes zero-gradient conditions for all variables. The remaining four surfaces are configured with zero

numerical fluxes, to mimic the 1D nature. The two-phase mixture spans a length of 1 m, and is initially filled with a gas phase consisting of $H_2/O_2/Ar$ at molar fractions of 1:1:4. While previous studies [21, 25, 26] have extensively examined the influence of gas composition on pulsating detonation characteristics, this work keeps it constant to isolate the effects of particle properties on hybrid detonation behavior. Notably, the H_2-O_2-Al system presents additional complexity due to the interaction between gas combustion products and Al particles. After hydrogen combustion, the resulting water vapor can further react with Al, leading to exothermic Al-water vapor reactions that further contribute to energy release [27]. This secondary reaction can influence detonation stability, wave propagation, and overall energy deposition [28], making the system more intricate than conventional gas-phase detonations.

The initial pressure and temperature are 0.2 atm and 300 K, respectively. The low pressure and high argon dilution are chosen to suppress excessive heat release and enhance the sensitivity of the system to detailed chemical kinetics, which facilitates clearer identification of reaction mechanisms and ignition characteristics, in line with the conditions in previous studies [16, 23]. A detailed hydrogen mechanism by Burke et al. [29] is applied, which has 13 species and 27 reactions. For the current gas mixture, the Half-Reaction Length (HRL) of the ZND structure for $H_2/O_2/Ar$ mixture is approximately $\Delta_{HRL} \approx 439$ μm. The Al particle induction zone typically exhibits a length scale one order of magnitude larger than that of the gas phase, primarily due to the substantial momentum and thermal response timescales with the particle phase [3]. Monodisperse and static Al particles are uniformly distributed across the domain at $t = 0$. For Al particles, the material properties are: initial temperature of 300 K, density of 2,700 kg/m^3 and isobaric heat capacity of 890 J/kg/K. The initial particle loading ranges from 0 to 600 g/m^3, and the particle diameter varies between 0.5 and 4 μm, covering a representative range of practical interest for aluminum-induced detonation studies [17, 30, 31]. Given the low particle volume fraction (typically below 0.02%), the inter-particle interactions, including collision effects, are reasonably neglected in the current analysis. Although the simulation employs a 1D configuration, the transverse dimensions (y and z directions) of the computational cells

remain relevant in the current modelling strategy as they determine the cell volume and consequently affect the particle number density. A computational parcel, representing identical particle properties (e.g., velocity, size, and temperature), is used in the simulations. Each CFD cell initially contains one parcel, and the particle number per parcel (n_p) varies with mass loading. The sensitivity of the mesh resolution and parcel number density is presented in Section A of the supplementary material. The results show that a cell size of 20 μm and a number density of 5.0×10^4/m are sufficient to capture the key characteristics of the hybrid detonation and hence will be used in this paper.

3. Numerical method

In our study, the compressible two-phase flow solver *DSRYrhoCentralFoam* [32, 33] is employed. It enables two-way coupling via run-time exchange of mass, momentum, and energy source terms. The gas phase is governed by the compressible Navier-Stokes equations, incorporating conservation laws for mass, momentum, energy, and species mass fractions, while the particle phase is tracked using a Lagrangian formulation. Recently, this solver has been applied to both single-particle combustion [34] and shock-induced combustion in Al-air mixtures [35]. Details of the two-phase governing equations are provided in Section B.1 of the supplementary material. Here, we introduce only the newly implemented sub-models, including the drag and surface reaction models for aluminum particles.

The quasi-steady drag force, recognized as the predominant force governing solid particle motion [36], is calculated as

$$\mathbf{F}_\mathrm{d} = \frac{18\mu_c}{\rho_d D_d^2}\frac{C_{D,Loth}Re_d}{24} m_d(\mathbf{u}_\mathrm{c} - \mathbf{u}_\mathrm{d}). \tag{1}$$

The improved drag law ($C_{D,Loth}$) recently developed by Loth et al. [37] is adopted, which reads

$$C_{D,Loth}(Re_d, Ma_d, Kn_d) = \begin{cases} \dfrac{C_{D,Kn_d,Re_d}(Re_d, Kn_d) + Ma_d^4 C_{D,fm,Re_d}(Re_d, Ma_d)}{1 + Ma_d^4}, & Re_d \le 45, \\ \dfrac{24}{Re_d}(1 + 0.15Re_d^{0.687})H_M + \dfrac{0.42C_M}{1 + 42500/Re_d^{1.16C_M} + G_M/Re_d^{0.5}}, & Re_d > 45. \end{cases} \tag{2}$$

The particle Knudsen number Kn_d is calculated from $Kn_d = \sqrt{\pi\gamma/2}\,(Ma_d/Re_d)$, where γ is the gas specific heat ratio, and the particle Mach number is $Ma_d \equiv |\mathbf{u}_c - \mathbf{u}_d|/c$, and c is the sound speed in the gas mixture. The expressions for C_{D,Kn,Re_d}, C_{D,fm,Re_d}, H_M, C_M, and G_M can be found in Section B.2 of the supplementary material. This formulation is based on extensive experimental data and particle-resolved direct numerical simulation results, offering broad applicability across both incompressible and compressible flows, as well as spanning regimes from the continuum to rarefied gas. This makes it particularly suitable for the present study, as submicron particles in a compressible background gas may enter the transitional regime ($0.01 < Kn_d < 10$) [38].

As the Al particles traverse the shock wave, they undergo rapid heating by the post-shock hot gas until reaching the melting point (933 K [39]). During this phase transition, the particle temperature remains constant until complete melting [40]. Following that, Al droplets undergo surface reactions with both oxygen and steam as oxidizers. Steam produced from hydrogen–oxygen combustion initiates additional exothermic reactions with aluminum particles [41, 42]. Developing accurate surface reaction models for aluminum under detonative conditions remains a significant challenge, particularly for hybrid H_2-O_2-Al mixtures, as suitable models are still scarce in the literature. In the current study, we employ a one-step global reaction mechanism as a practical approach, with future model improvements contingent upon the availability of more comprehensive experimental data. The reactions are [12]: $4\mathrm{Al(l)} + 3\mathrm{O_2} \rightarrow 2\mathrm{Al_2O_3(s)}$ and $2\mathrm{Al(l)} + 3\mathrm{H_2O} \rightarrow \mathrm{Al_2O_3(s)} + 3\mathrm{H_2}$. It is assumed that the aluminum oxide (Al_2O_3) produced during combustion deposits on the particle surface. The particle diameter treatment follows the methodology described in our recent study on aluminum particle combustion [34]. Previous studies [43, 44] have demonstrated that AlO production becomes significant when the particle temperature exceeds the decomposition threshold, which can be estimated as [30]

$$T_{dec} = \frac{1}{2.5051\times10^{-4} - 1.4132\times10^{-5}\times\ln(p_{atm})}, \tag{3}$$

where p_{atm} is normalized by the standard atmospheric pressure (101,325 Pa). This results in a decomposition temperature of approximately 4,500 K, significantly higher than the maximum particle

temperature observed in this study (~3,500 K). Therefore, AlO formation is not considered in current simulations.

For the particle surface reaction model, we adopt a hybrid model [5], which combines surface kinetic oxidation and diffusion reaction under detonative conditions. The mass reaction rate is

$$\dot{m}_{Al,HTR} = -A_{d,Al} C_{oxi} \frac{\nu_{Al} W_{Al}}{\nu_{oxi} W_{oxi}} \frac{k_d k_s}{k_d + k_s}, \quad (4)$$

where $A_{d,Al}$ is the effective Al droplet diameter, ν the stoichiometric coefficient, W the molecular weight, and C_{oxi} the molar concentration of the oxidizing gas. The subscript *oxi* denotes oxidizer, which may refer to either oxygen or steam. In this study, we adopt C_{oxi} = 1.0 for oxygen and C_{oxi} = 0.6 for steam, based on Beckstead's correlation fitted to nearly 400 data points on single-particle burning times in various oxidizer environments [41]. The diffusion rate coefficient k_d is

$$k_d = \frac{\nu_{oxi} W_{oxi}}{\nu_{Al} W_{Al}} \frac{\rho_d D_{d,Al}}{2 C_{total} K D_{d,0}^2} (1 + 0.276 Re^{1/2} Pr^{1/3}), \quad (5)$$

where K = 4×10^6 s/m^2, and C_{total} is the molar concentration of gas mixture. The kinetic surface reaction coefficient is

$$k_s = k_0 e^{-E/RT_s}, \quad (6)$$

where the pre-exponential factor is k_0 = 1,200 kg·m/mol·s, and the activation energy is E = 71.1 kJ/mol. The surface temperature is defined as $T_s = (T_c + T_d)/2$, accounting for thermal nonequilibrium between the particle and the surrounding gas. The particle heat release rate is $\dot{q}_{Al,oxi} = \dot{m}_{Al,oxi} h_{Al,oxi}$, where $h_{Al,oxi}$ is the heat from surface reaction, taking 3.1×10^7 J/kg for Al-O_2 reactions and 1.8×10^7 for J/kg for Al-H_2O reactions [5]. Several studies [30, 40, 45] confirm that this model inherently transitions between the kinetic-limited and diffusion-limited burning regimes without requiring an arbitrary ignition temperature. Therefore, it is well-suited for predicting transient processes, such as detonation initiation, abrupt deflagration-to-detonation transition (DDT), and detonation instability [5].

The current solver has been extensively validated and successfully applied to various two-phase detonation systems, including hydrogen-inert particle [46], methane-char particle [7], and coal particle detonations [6]. In this study, it is further validated against aluminum-air detonation experiments [47-49]. Fig. 2 presents the predicted detonation speeds as a function of aluminum particle loading under

atmospheric conditions of 300 K and 2 atm. The results demonstrate that the solver can reasonably predict the detonation speeds for loadings from 200 to 800 g/m^3. Notably, when the loading is reduced to 100 g/m^3 or increases up to 850 g/m^3, the detonation fails.

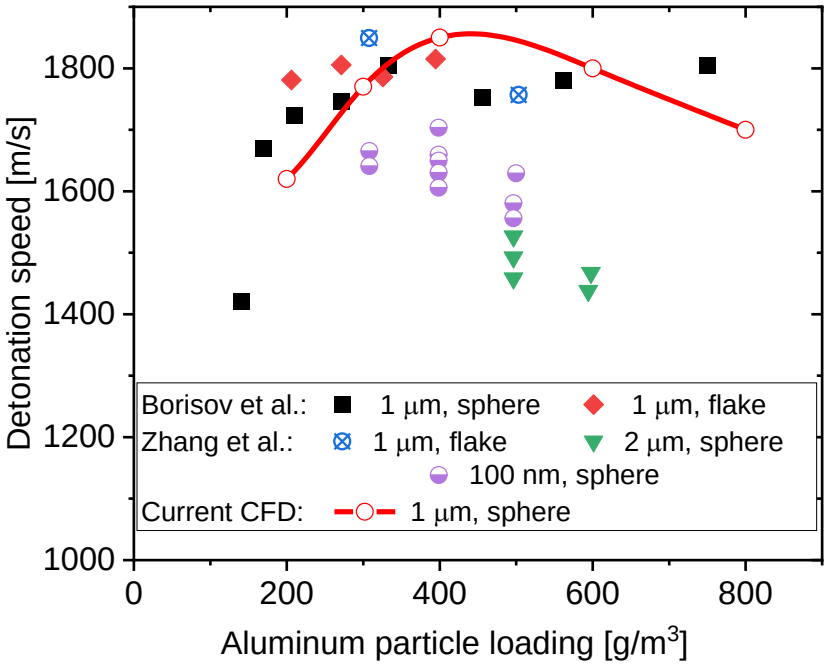

Fig. 2 Change of detonation speed with particle loading for aluminum-air mixture. The experiment data are reported from Borisov et al. [47] and Zhang et al. [48, 49].

4. Results and discussion

4.1 Mode of detonation propagation

The hybrid detonation propagation characteristics under different particle loadings (η) are presented in Fig. 3. Figure 3(a) illustrates the spatial evolution of detonation speed (D), whereas Fig. 3(b) displays the corresponding average speeds across different particle loadings. The Chapman-Jouguet speed, 1,583 m/s, at the particle-free case (η = 0) is indicated by the dashed line in Fig. 3(a), serving as the reference for normalization. Figure 4 shows the evolutions of peak heat release rate (HRR), gas temperature, and particle volume fraction at the aluminum reaction front (RF), along with the particle induction length, as functions of particle loading. Evidently, the detonation propagation exhibits four regimes based on speed characteristics in Fig. 3(b), each demonstrating unique combustion dynamics.

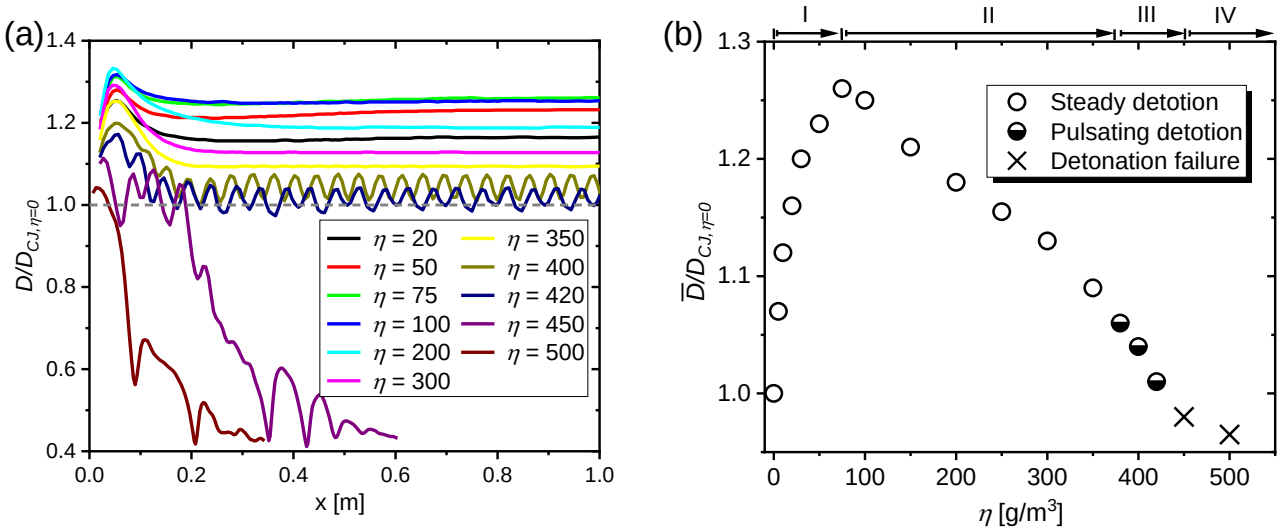

Fig. 3 (a) Evolution of detonation propagation speed for different particle loadings; (b) Change of average detonation speed with the particle loading. The particle diameter is D_d = 1 μm.

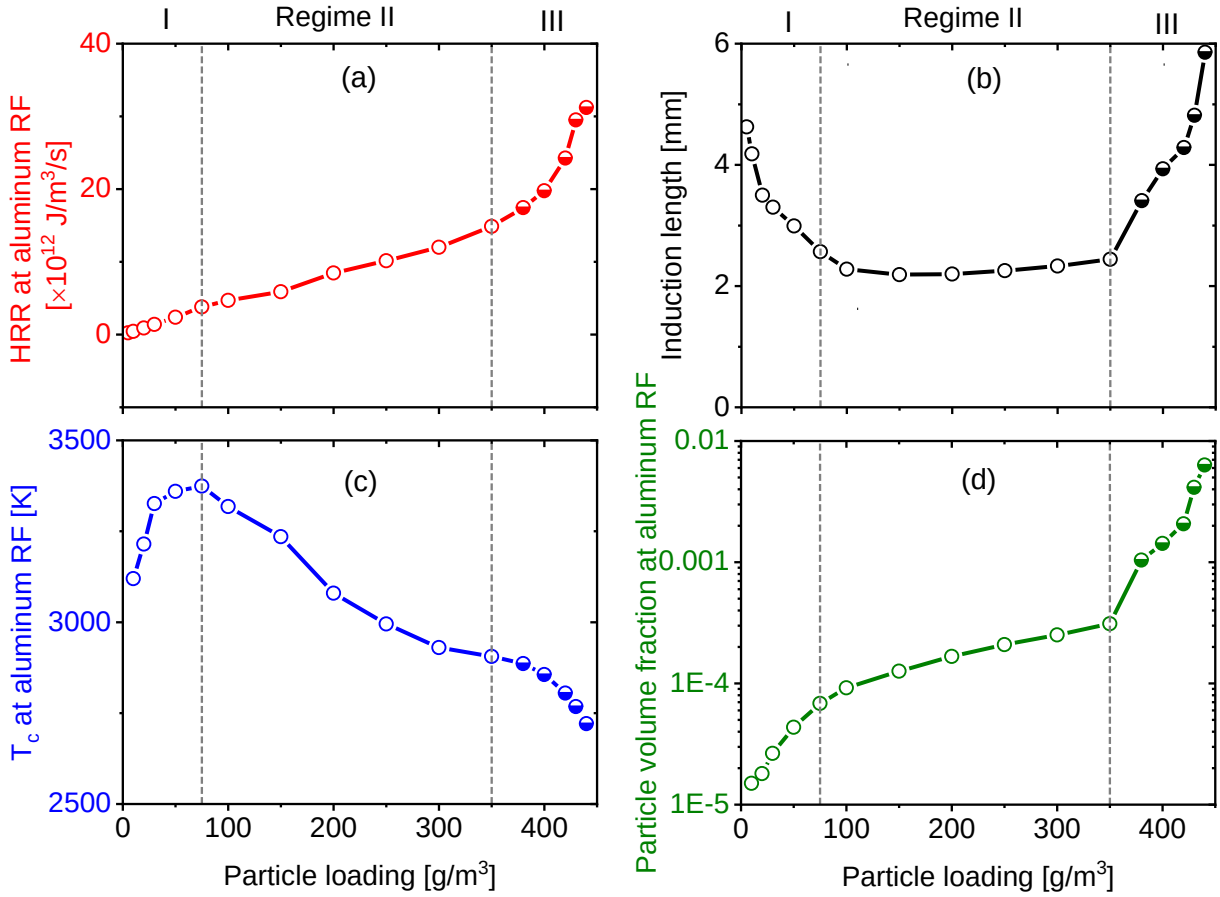

Fig. 4 Evolutions of aluminum (a) peak heat release rate (HRR), (b) induction length, (c) gas temperature at aluminum reaction front (RF), and (d) particle volume fraction at aluminum RF, as functions of particle loading (η).

In Regime I ($0 < \eta < 75$ g/m^3), the detonation wave establishes steady propagation after an initial transition length of approximately 0.2 m. The degree of speed enhancement (i.e., the degree of

overdrive [26], $D/D_{CJ,\eta=0}$) increases rapidly with particle loading. This trend is attributed to two factors: the increase in aluminum HRR and the reduction in aluminum induction length, as shown in Figs. 4(a) and 4(b), respectively. Within this particle fuel-lean regime, both the gas temperature and particle volume fraction at the aluminum reaction front increase rapidly, indicating enhanced particle combustion intensity.

In Regime II ($75 < \eta < 350$ g/m^3), the detonation speed gradually decreases with particle loading, resulting in a reduction in gas temperature at the RF. However, due to the increased particle concentration behind the leading shock (see Fig. 4d), the peak HRR continues to increase nearly linearly, while the particle induction length remains relatively unchanged.

As the particle loading increases further, the system transitions into Regime III ($350 < \eta < 450$ g/m^3), characterized by a pulsating propagation mode. In this regime, the average detonation speed ($\bar{D}$) continues to decline with increasing particle loading. Although the peak aluminum HRR still increases, the induction length also grows rapidly, indicating a tendency for the aluminum reaction front to decouple from the shock front. This decoupling is primarily attributed to a drop in gas temperature and the rapid accumulation of particles near the aluminum reaction front, as shown in Figs. 4(c) and 4(d), respectively.

At higher particle loadings ($\eta > 450$ g/m^3), the detonation wave loses its self-sustaining capability, resulting in failure, defined as Regime IV. This transition is exemplified by the cases with $\eta = 450$ and 500 g/m^3, as shown in Fig. 3(a).

The characteristics of hydrogen combustion, specifically the gas peak HRR and induction length, are presented in Section C of the supplementary material. The results reveal two key differences compared to those of aluminum particle combustion. First, the peak HRR and induction length are both much lower than those of Al particles. Second, these parameters remain nearly constant across different particle loading conditions, indicating that gas-phase combustion is far less sensitive to Al particle loading variations. This difference arises because most of the hydrogen combustion heat is released prior to particle ignition.

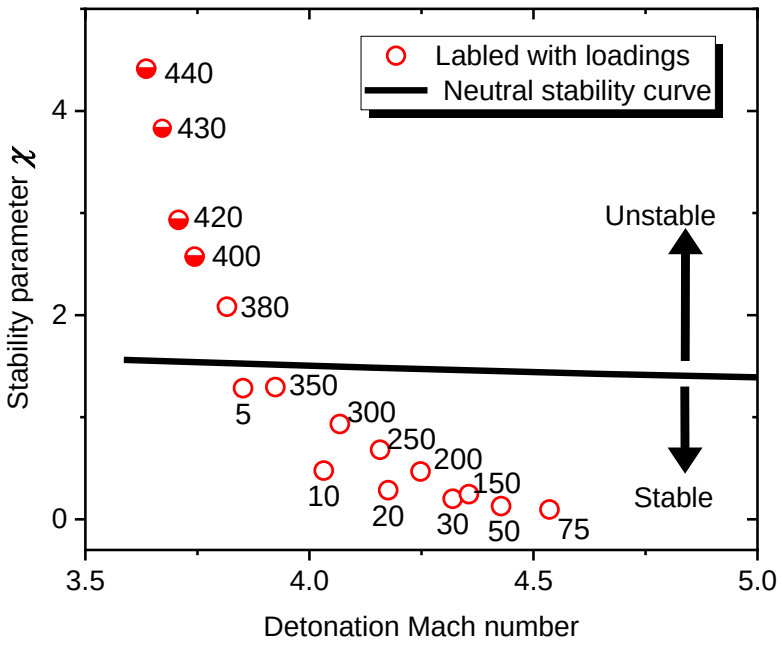

Fig. 5 Stability parameter versus detonation Mach number for the cases shown in Fig. 3. The solid neutral stability curve is taken from Ng et al. [23]. The number near the symbol is aluminum particle loading with unit of g/m^3.

Following the stability parameter χ proposed by Ng et al. [23],

$$\chi \equiv \varepsilon_I \frac{\Delta_{IL,Al}}{\Delta_{RL,Al}}, \tag{7}$$

where ε_I is the reduced effective activation energy, defined as $\varepsilon_I = E_I/T_s$, with E_I being the global activation energy and T_s the temperature jump across the leading shock. $\Delta_{IL,Al}$ and $\Delta_{RL,Al}$ denote the induction and reaction lengths of aluminum particles, respectively. The computed values of ε_I range approximately from 4 in the particle-free case to 10 in the pulsating case in Fig. 3. Fig. 5 summarizes the cases by plotting the stability parameter χ along with the neutral stability curve proposed by Ng et al. [23]. The detonation Mach number is calculated based on the ratio $D/D_{CJ,\eta=0}$ shown in Fig. 3, where $D_{CJ,\eta=0}$ corresponds to a Mach number 3.6. Notably, the current one-dimensional hybrid detonation states also align well with this universal neutral stability curve. As the particle loading increases from 5 to 75 g/m^3, the decreasing χ indicates enhanced detonation stability. Further increases in loading lead to a rise in χ, suggesting a reduction in wave stability. Specifically, when the loading exceeds 380 g/m^3, the elevated χ surpasses the neutral stability threshold, ultimately triggering the pulsating propagation behavior observed in Regime III.

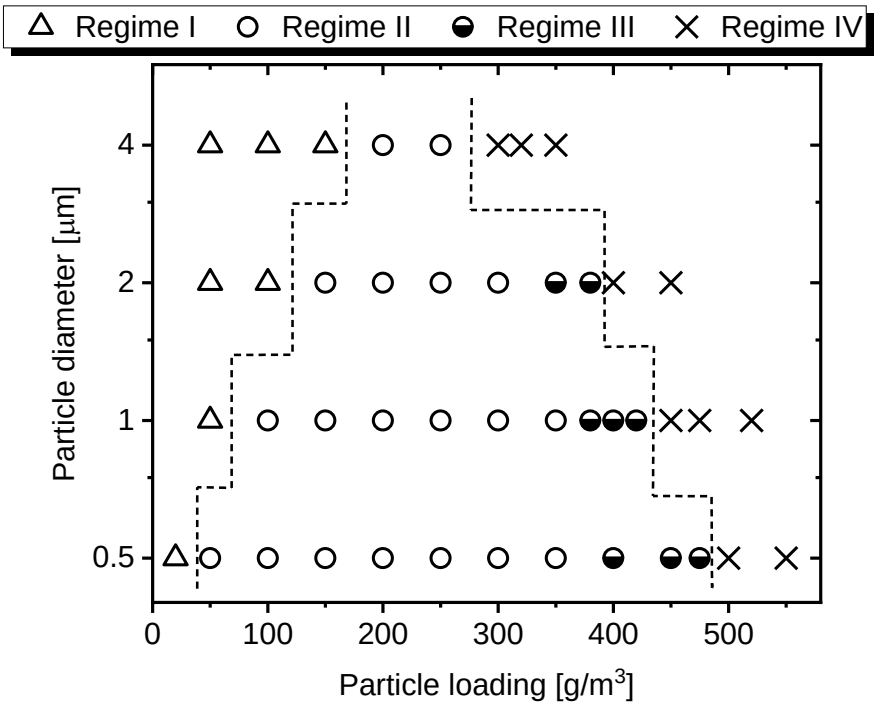

Fig. 6 Diagram of detonation Regime I to IV: particle diameter versus particle loading.

Figure 6 presents a comprehensive phase diagram illustrating different propagation regimes as functions of particle loading and particle diameter. The results show a clear dependence of regime transitions on particle size: as diameter increases from 0.5 to 4 μm, the critical particle loading between Regime I and II rises from ~40 g/m^3 to 175 g/m^3, marked by the left dashed line in Fig. 6. This is because for larger particles, the reduced heat transfer efficiency due to their smaller specific surface area results in longer induction zones. As a result, larger particles require higher HRR, which is achieved through increased particle loading to compensate for the extended induction lengths. Notably, pulsating propagation (Regime III) occurs only when the particle diameter is relatively small. In contrast, larger particles under high loading conditions are more likely to cause detonation failure due to the loss of self-sustaining propagation. The critical particle loading threshold for detonation failure exhibits an inverse correlation with particle diameter, as indicated by the right dashed line in Fig. 6. This fundamental inverse correlation between particle size and detonation stability has been consistently demonstrated and validated in previous experimental and numerical studies [17, 49, 50].

4.2 Steady detonation

In this section, we focus on the steady detonation propagation in Regime I and II. When the detonation wave reaches a steady state, the post-shock structure remains stable in the shock frame. We analyze a representative case with D_d = 1 μm and η = 100 g/m^3 in Fig. 7, which displays the post-shock distributions of pressure, gas and particle temperatures, heat release rates, and molar concentrations of various species.

As shown in Fig. 7(a), the hydrogen reaction front, identified by the peak HRR at point 2, propagates ahead of the Al reaction front (point 3) behind the shock front (point 1). Figure 7(b) reveals a two-stage temperature rise in the post-shock gas phase: the first temperature increase (~2,900 K) is primarily driven by hydrogen combustion, while the second one (~3,800 K) results mainly from Al particle combustion, as confirmed by two peaks in the total HRR ($\dot{q}_{HRR,total}$) profile in Fig. 7(c). Notably, the heat contribution from Al-O_2 reactions exceeds that from Al-H_2O reactions, even though the O_2 fraction is lower than that of H_2O. Interestingly, within the particle reaction zone, the thermal effect of gas-phase reactions transitions from being exothermic to endothermic. This shift results from the rapid depletion of water vapor (Fig. 7d), which is consumed by particle surface reactions. To investigate this phenomenon, a detailed reaction pathway analysis was conducted using Cantera, focusing on elementary reactions involving the H radical. Details of the analysis are provided in Section D of the supplementary material. The results indicate that the primary contributors to the endothermic effect are the following H_2O decomposition reactions: R7: $H_2O + M <=> H + OH + M$ and R3: $H + H_2O <=> H_2 + OH$. Behind the Al reaction front, the pressure gradually decreases, characterizing the expansion zone of the hybrid detonation.

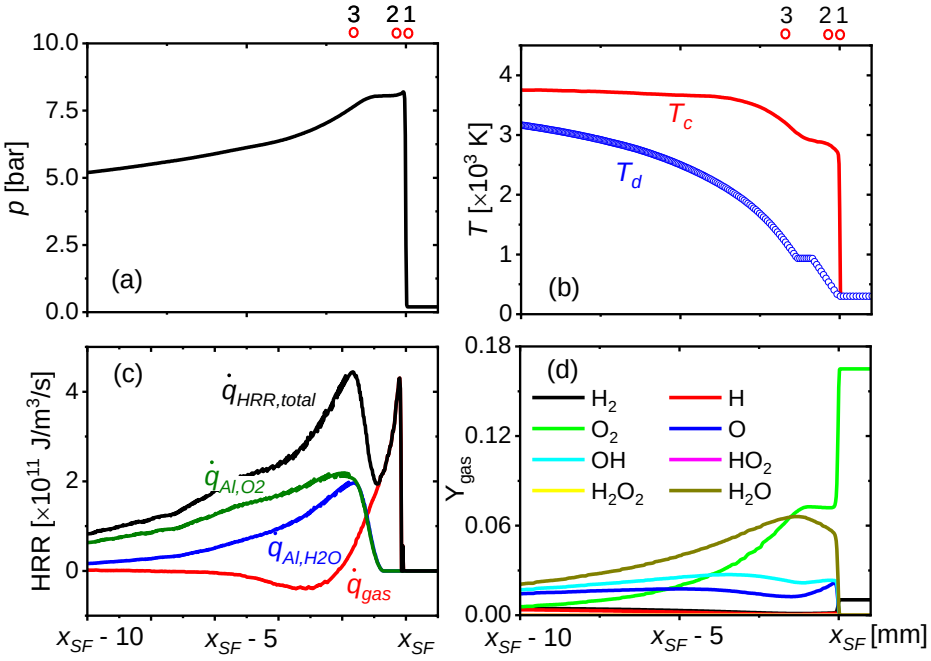

Fig. 7 Post-shock distributions of (a) pressure, (b) gas and particle temperature, (c) heat release rate, and (d) molar concentrations of various species. The particle diameter is 1 μm, and the particle loading is 100 g/m^3. Point 1 correspond to the shock front (SF); and points 2 and 3 are respectively for reaction fronts of hydrogen and aluminum.

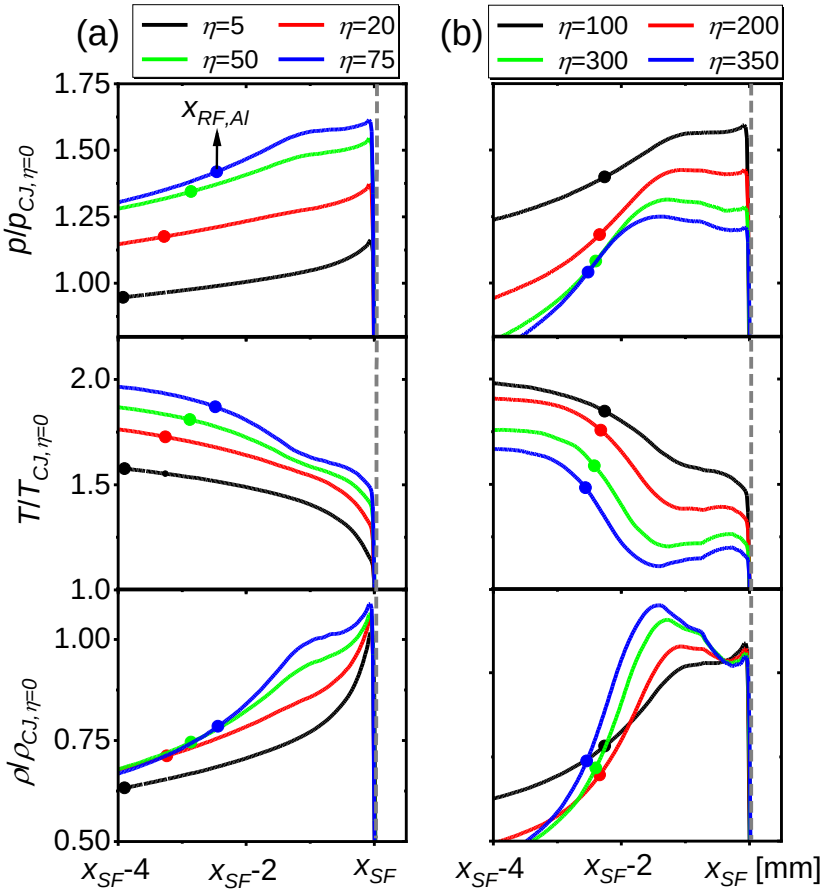

Fig. 8 Distributions of normalized pressure (top), gas temperature (middle) and density (bottom) for different particle loadings: (a) Regime I, (b) Regime II. Solid symbols represent the locations of Al HRR peak, $x_{RF,Al}$.

Figure 8 presents the profiles of pressure, gas temperature, and density behind the shock front with various particle loadings. For Regime I (5-75 g/m^3), the von Neumann spike pressure increases rapidly with particle loading, primarily due to the substantial rise in gas temperature. This intensification is driven by the increase in the Al HRR peak and the decrease in the Al induction length, as seen from the solid symbols in Fig. 8(a). Both pressure and gas density exhibit gradual decay profiles downstream of the shock wave, indicating an immediate expansion region. This corresponds to the single-front detonation (SFD) structure, following the classification proposed by Veyssiere [3], wherein the von Neumann pressure aligns with the peak pressure. It is noteworthy that a similar single-pressure-peak structure was observed in recent one-dimensional Al-air detonation study [18]; however, their reported pressure peak slightly trails behind the shock front. The reason for this discrepancy is primarily attributed to the effect of hydrogen combustion heat release.

For Regime II (75-350 g/m^3) in Fig. 8(b), the flow field undergoes a significant transition, evolving into a unique quasi-double-front detonation (quasi-DFD) structure. This structure is characterized by the formation of a distinct compression zone located behind the shock front but ahead of the Al reaction front (indicated by the solid symbol in Fig. 8b). Spatially, this compression zone resides within the particle induction zone. This transitional structure only occurs for small, micron-sized particles. As the particle diameter increases to around 4 μm, the quasi-DFD structure further develops into a typical DFD structure [3, 18], characterized by two distinct pressure peaks. This transition is attributed to the elongation of the particle induction zone with increasing particle size. Additional details on this transition are provided in Section E of the supplementary material.

To elucidate the formation mechanisms underlying the two distinct pressure profiles observed in Fig. 8, one-dimensional gas-dynamic flow theory [51] is employed for quantitative analysis. The hybrid detonation structure of H_2-Al mixtures results from complex interactions among various physical and chemical processes, including hydrogen combustion, interphase heat convection, particle combustion, and interphase momentum transfer. These effects can be decoupled and quantified using the following equations [30]:

$$\begin{cases} -\dfrac{1}{p}\dfrac{\mathrm{d}p}{\mathrm{d}x}\Big|_{\mathrm{H2,react}} = \dfrac{\gamma Ma^2}{Ma^2-1}\dfrac{\dot{q}_{H2}}{\rho c_p T}\dfrac{1}{U}, \\ -\dfrac{1}{p}\dfrac{\mathrm{d}p}{\mathrm{d}x}\Big|_{\mathrm{Al,conv}} = \dfrac{\gamma Ma^2}{Ma^2-1}\dfrac{S_{Al,conv}}{\rho c_p T}\dfrac{1}{U}, \\ -\dfrac{1}{p}\dfrac{\mathrm{d}p}{\mathrm{d}x}\Big|_{\mathrm{Al,react}} = \dfrac{\gamma Ma^2}{Ma^2-1}\left(\dfrac{S_{Al,react}}{\rho c_p T}+\dfrac{S_{mass}}{\rho}\right)\dfrac{1}{U}, \\ -\dfrac{1}{p}\dfrac{\mathrm{d}p}{\mathrm{d}x}\Big|_{\mathrm{mom}} = \dfrac{\gamma Ma^2[1+(\gamma-1)Ma^2]}{Ma^2-1}\dfrac{S_{mom}}{\rho U}\dfrac{1}{U}. \end{cases} \tag{8}$$

Here U and Ma represent the relative velocity and Mach number in the shock coordinate system, respectively. γ is the specific heat ratio, $\dot{q}_{H2}$ the gas-phase HRR, $S_{Al,conv}$ the interphase heat convection rate, $S_{Al,react}$ the Al particle combustion HRR, S_{mass} the interphase mass transfer rate, and S_{mom} the interphase momentum transfer rate. Two representative cases with particle loadings of 30 and 300 g/m^3, corresponding to Regimes I and II respectively, are selected for detailed analysis. Figure 9 presents post-shock distributions of pressure, the net value of $-(\mathrm{d}p/\mathrm{d}x)/p$, and the four separate contribution terms in Eq. (8).

When η = 30 g/m^3, the pressure behind the leading shock continuously decreases, yielding a consistently negative net value of $-(\mathrm{d}p/\mathrm{d}x)/p$. This is primarily driven by sequential combustion effects from H_2 and Al particles, as illustrated in Fig. 9(b). Before the initiation of Al particle surface reactions, the negative contribution from hydrogen combustion surpasses the combined positive contributions of interphase momentum transfer and heat convection. As a result, an immediate pressure decrease follows the shock front. Apparently, particle combustion significantly elongates the reaction zone and primarily contributes to the formation of the expansion region in the hybrid mixture.

When η = 300 g/m^3 in Fig. 9(c), a significant increase in interphase momentum and heat transfer occurs prior to the initiation of particle surface reactions, surpassing the effects of hydrogen combustion. Consequently, the net contribution from the four terms becomes positive immediately downstream of the shock, resulting in the formation of a compression region. As the particle diameter increases, the particle induction length extends substantially, transforming this quasi-DFD structure into a typical DFD structure characterized by two distinct pressure peaks, as extensively investigated in recent Al-air detonation studies [18]. Upon initiation of particle surface reactions, the Al combustion

effect rapidly increases, causing the net value of $-(\mathrm{d}p/\mathrm{d}x)/p$ to drops below zero and leading to the formation of an expansion region. In this scenario, hydrogen combustion plays a relatively minor role in shaping the pressure profile, with the particle phase predominantly governing both the compression and expansion zones. Thus, such a hybrid detonation inherently constitutes a heterogeneous detonation [35].

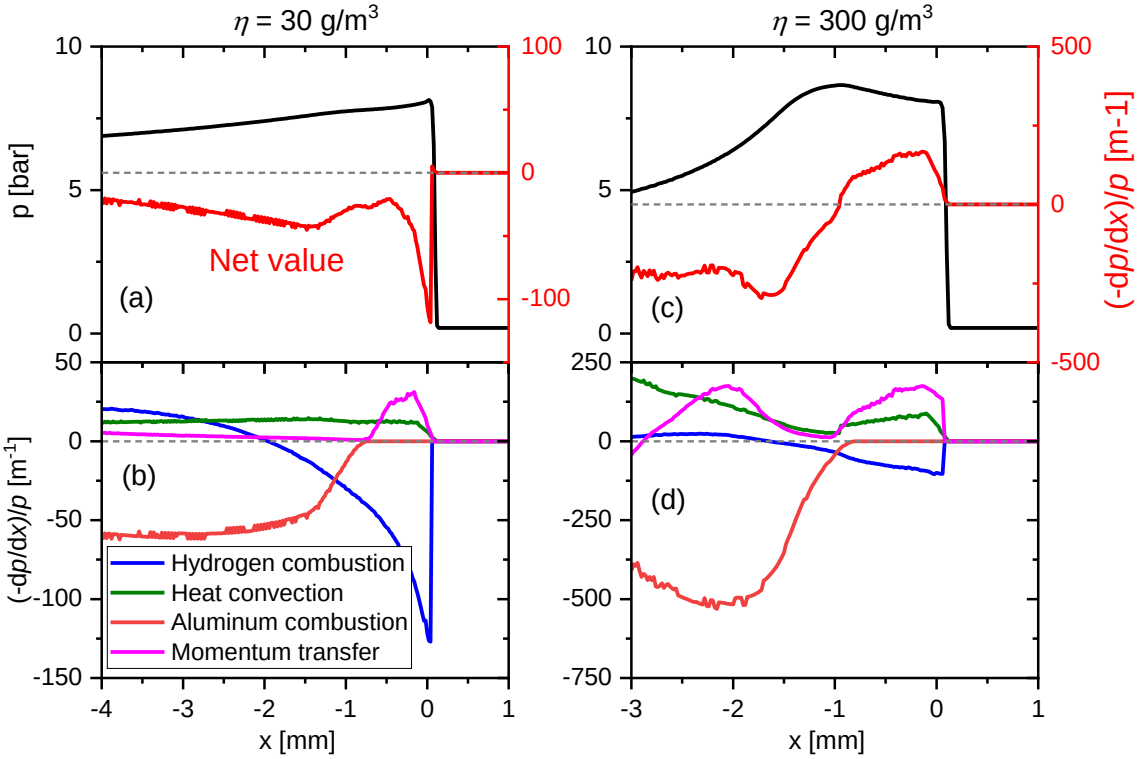

Fig. 9 Upper panels: pressure profile and net value of $-(\mathrm{d}p/\mathrm{d}x)/p$. Lower panels: Separate contributions of hydrogen combustion, interphase heat convection, aluminum particle combustion, and momentum transfer to the pressure profile. Particle loading is 30 g/m^3 in (a) and (b), and 300 g/m^3 in (c) and (d).

4.3 Pulsating detonation

Although pulsating propagation modes have previously been observed in one-dimensional Al-air [18] and Al-C_2H_2-air [12] detonations, detailed analyses of the underlying mechanisms driving such pulsations have not been provided. This section investigates the fundamental mechanisms governing such pulsating behavior in hybrid detonation system. To elucidate these mechanisms, a representative case with D_d = 2 μm and η = 380 g/m^3 has been selected.

Figure 10 presents the temporal evolution of shock speed, integrated heat release rate from aluminum combustion ($\dot{Q}_{Al,comb}$), hydrogen combustion ($\dot{Q}_{H2,comb}$), and interphase heat convective

exchange ($\dot{Q}_{conv}$). The results reveal that the pulsating behaviors of the shock speed primarily originate from oscillations in the heat release from the particle phase. In contrast, the integrated heat release from hydrogen combustion remains relatively stable.

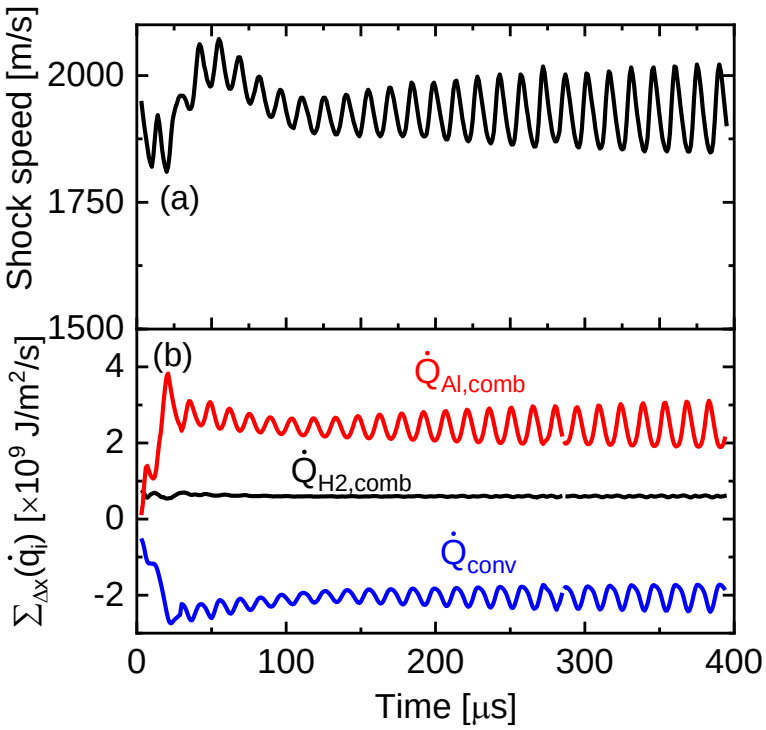

Fig. 10 Evolutions of (a) shock speed and (b) integrated heat transfer rate. The particle diameter and mass loading are 2 μm and 380 g/m^3, respectively.

Figure 11 presents the *x*-*t* diagrams of four critical parameters - pressure, gas temperature, gas momentum, and energy source terms - in the shock frame. As shown in Fig. 11(a), the system generates periodic strong compression waves that originate from the Al reaction front and propagate upstream towards the shock front, while simultaneously producing weaker compression waves that travel downstream into the expansion region. Both wave systems exhibit pulsation patterns synchronized with the Al reaction front, indicating a strong coupling between the particle combustion dynamics and wave propagation characteristics. The particle induction zone, defined as the region between the shock front and Al reaction front, is characterized by simultaneously elevated pressure (Fig. 11a) and reduced temperature (Fig. 11b) compared to the downstream expansion region. Notably, substantial negative values of interphase momentum loss ($\mathbf{S}_{\mathrm{mom}}$, Fig. 11c) are observed within this zone, caused by drag forces resulting from the large velocity difference between the two phases [35]. This region also

exhibits a negative convective heat transfer rate (Fig. 11d). Immediately downstream, strong heat

Fig. 11 Temporal evolution of the distributions of (a) pressure, (b) gas temperature, (c) momentum source term, and (d) energy source term in the frame moving with the shock front. The particle diameter is 2 μm, and the particle loading is 380 g/m^3.

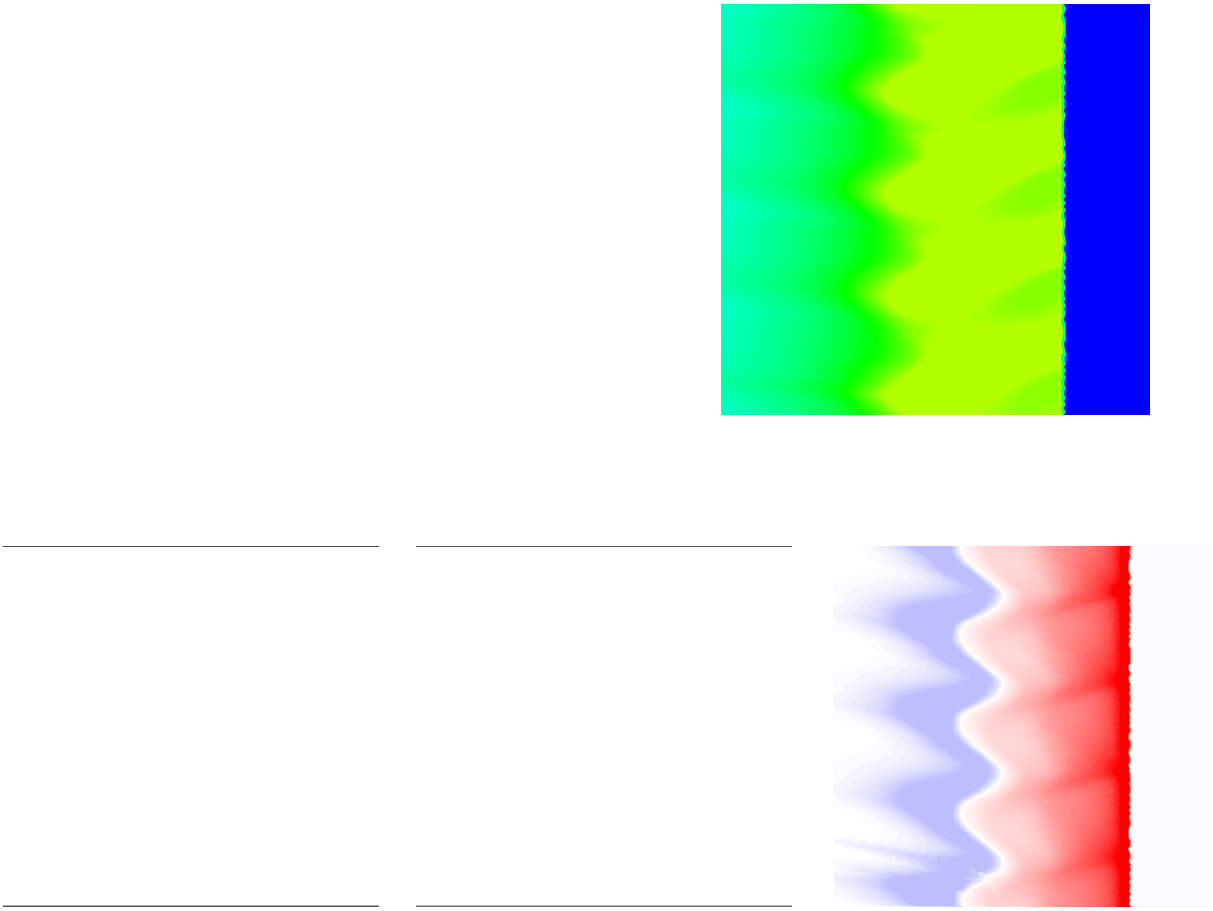

Fig. 12 Temporal evolution of (a) shock speed, (b) local heat release rate at Al reaction front (RF), (c) pressure, (d) gas density, (e) gas temperature, and (f) gas heat release rate distributions in the frame moving with the shock front.

Figure 12 presents complementary *x*-*t* diagrams illustrating the temporal evolution of shock speed, local HRR at the Al reaction front, the distributions of pressure, gas density, gas temperature, and gas-phase HRR. A complete pulsation cycle occurs between 218 and 232 μs, as marked by the two horizontal lines. The acceleration stage (218-226 μs) is characterized by a progressive increase in shock speed from 1,885 to 1,998 m/s. This acceleration initiates at the location corresponding to maximum HRR at the Al reaction front in Fig. 12(b). The intense energy release at this location generates a high-amplitude pressure wave that propagates upstream toward the shock front, which is marked by the red arrow in Fig. 12(c). This upstream-propagating pressure wave serves as the primary mechanism driving the observed shock acceleration through wave reinforcement [26]. At 226 μs (i.e., the horizontal dashed line), the interaction of the pressure wave with the shock front generates a

localized high-temperature region (2,805 K), as labeled in Fig. 12(e). This triggers the formation of a contact discontinuity (i.e., entropy wave [52]) with distinct density (Fig. 12d) and temperature (Fig. 12e) discontinuities. As the contact discontinuity propagates downstream from 226 to 232 μs, it marks the onset of the deceleration stage. Its subsequent interaction with the original Al reaction front raises the local temperature, accelerating chemical reaction kinetics and amplifying the HRR, thereby triggering the next pulsation cycle.

Furthermore, Fig. 12(f) reveals that the interface between heat absorption and release regions associated with hydrogen combustion is spatially localized near the Al reaction front. This interface demonstrates temporal synchronization with the pulsation characteristics of the Al reaction front, as evidenced by their phase-locked behavior. The observed correlation is mediated through the oscillatory gas temperature field near the Al reaction front, demonstrating the thermal coupling between gas-phase and particle-phase combustion processes.

Table 1 Summary of oscillation patterns in shock-induced combustion, gaseous detonation, and hybrid detonation systems.

Category		**Stagnation streamline before blunt body**	**1D homogeneous detonation**	**1D hybrid detonation**
Combustion system		Shock-induced combustion	Hydrogen-air	Hydrogen-oxygen-argon + aluminum particles
Oscillation modes	Regular regime	✓	✓	✓
	Large-disturbance regime	✓	✓	-
One oscillation cycle of regular regime	Accelerating stage	**Compression wave:** reaction front → shock front		
	Decelerating stage	**Contact discontinuity:** shock front → reaction front		
Key influencing factors		Projectile radius [53]; activation energy [54]	Degree of overdrive [26]; activation energy [55]	Particle loading; particle diameter; particle activation energy

Table 1 summarizes the oscillation patterns observed in three combustion systems: shock-induced combustion around blunt bodies [52, 56], one-dimensional hydrogen-air detonations [20, 26], and

current two-phase hybrid system. There are generally two kinds of oscillation modes: the regular regime and the large-disturbance regime. In the regular regime, the acceleration stage is characterized by upstream-propagating compression waves from the reaction front to the shock front, while the deceleration stage features downstream-traveling contact discontinuities from the shock front to the reaction front, as schematized in Fig. 12. Although the pulsating behavior observed in the three combustion systems appears similar at the macroscopic level, their underlying driving mechanisms differ fundamentally. In shock-induced combustion around blunt bodies, oscillations arise from the complex interaction between gas-phase reactions and the solid body geometry [53]. In unsteady hydrogen–air detonations, the instability primarily originates from the intrinsic properties of highly exothermic, chain-branching reaction mechanisms [23]. In contrast, the pulsations in the present hybrid detonation system are driven by periodic heat release from particle-phase combustion, modulated by particle accumulation behind the shock front.

In the large-disturbance regime, the reaction front propagates upstream, eventually overtaking and directly interacting with the shock front, resulting in pulsed shock acceleration [26, 54]. Notably, this regime is absent in the current hybrid detonation system. This absence can be attributed to the inherent physical constraints of particle-laden systems: the direct interaction between the Al particle reaction front and the shock front is unlikely due to finite induction zone lengths. These finite lengths are maintained by the substantial momentum and thermal response timescales of the particulate phase. This fundamental difference highlights the unique characteristics present in hybrid detonation systems compared to purely gaseous detonations.

Furthermore, Table 1 provides a summary of key factors influencing wave propagation instability across different detonative combustion systems. In shock-induced combustion around blunt bodies, experimental and numerical studies have demonstrated that increased projectile radius [53] and reduced activation energy [54] significantly enhance instability. For one-dimensional hydrogen-air detonations [26], the degree of overdrive (f) serves as a crucial parameter for characterizing pulsation modes, with smaller f values correlating with increased instability. In the current hybrid detonation

simulations, we identify three primary factors for wave stability: (1) increased particle loading, (2) larger particle diameter, and (3) elevated particle activation energy. These parameters collectively contribute to the transition from stable to unstable propagation modes.

4.4 Discussion on particle combustion

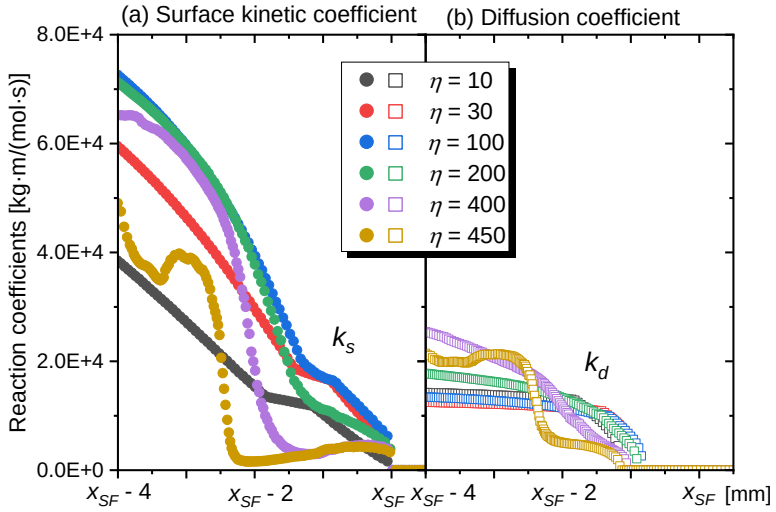

Fig. 13 Spatial distributions of (a) surface kinetic coefficient k_s and (b) diffusion coefficient k_d behind the shock front with different particle loadings. Particle diameter is 1 μm.

The preceding analysis is primarily focused on gas dynamics; this section turns to the characteristics of particle combustion. The Al mass reaction rate, governed by Eq. (4), is controlled by two competing factors: the surface-kinetic coefficient (k_s) and the diffusion coefficient (k_d). The overall reaction rate is determined by the rate-limiting coefficient, corresponding to the smaller one. Figure 13 presents the spatial distributions of k_s and k_d for different particle loadings with particle diameter 1 μm. Here, only the coefficients associated with oxygen are shown, as Al-O_2 reactions dominate under high particle loading conditions. However, it is worth noting that the trends of the corresponding coefficients for Al-H_2O reactions closely follow those presented in Fig. 13.

As shown in Fig. 13(a), the surface-kinetic coefficient exhibits significant sensitivity to particle loading. In Regime I ($0 < \eta < 100$ g/m^3), k_s increases rapidly with particle loading, primarily due to the rise in particle surface temperature (T_s), see Fig. 14(a). This correlation can be explained with the Arrhenius-type temperature dependence of k_s described in Eq. (6). In contrast, in Regimes II and III

(η > 100 g/m^3), k_s gradually decreases as T_s declines progressively at higher loadings. Compared to k_s, the diffusion coefficient (k_d) exhibits significantly less sensitivity to variations in particle loading.

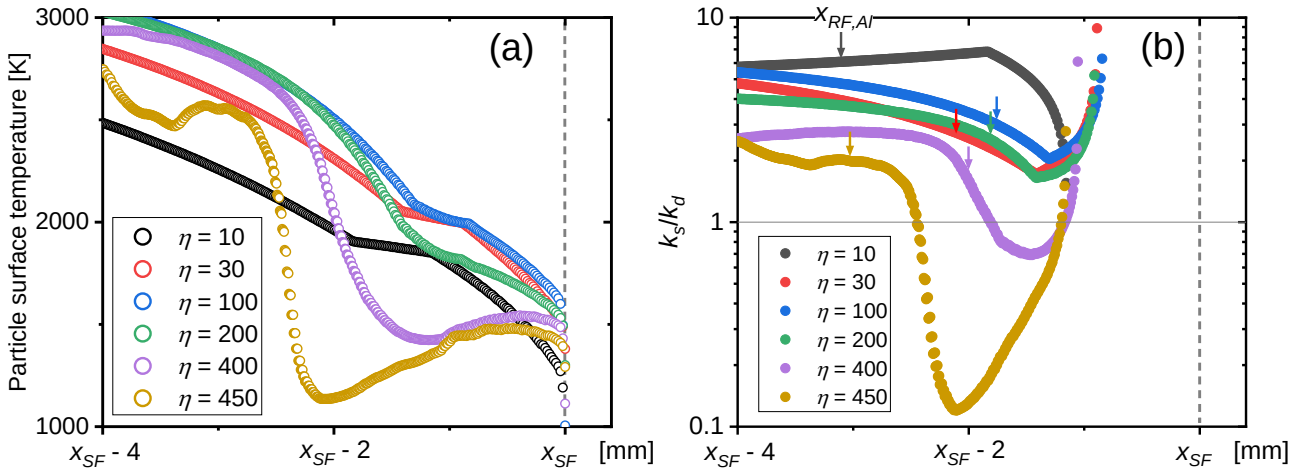

Fig. 14 Distributions of (a) particle surface temperature, and (b) ratio of surface kinetic coefficient k_s to diffusion coefficient k_d. Arrows represent the positions of aluminum reaction front.

To quantitatively evaluate the contributions of surface kinetics versus diffusion processes in particle combustion, we analyze the ratio of surface-kinetic coefficient to diffusion coefficient (k_s/k_d), with its spatial distribution presented in Fig. 14(b). The arrows mark the positions of the Al reaction front. A ratio exceeding 1.0 indicates that diffusion plays a dominant role in combustion, whereas values below 1.0 reflect the greater influence of surface kinetics. Across three Regimes, as the particle loading increases, the ratio k_s/k_d within the particle induction zone ($x_{RF,Al} < x < x_{SF}$) generally decreases, demonstrating the growing dominance of surface-kinetic reactions. Particularly noteworthy is the case of η = 450 g/m^3 in Regime III, where the ratio undergoes a substantial reduction, falling below unity across most of the induction zone. Consequently, particle combustion within this region becomes surface-kinetic-limited. It is worth highlighting that a similar kinetic-limited zone was observed during the transition stage of deflagration-to-detonation transition (DDT) in an Al–air detonation study [5]. However, once stable detonation was established, particle temperatures rose rapidly, leading to predominantly diffusion-limited reactions throughout most of the Al reaction zone, consistent with the present findings. Collectively, these results underscore the critical influence of temperature-dependent surface-kinetic reactions in governing detonation wave stability.

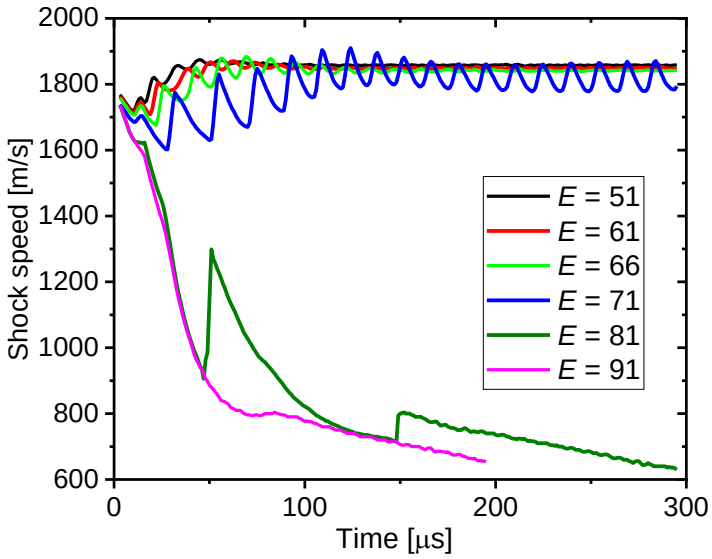

Fig. 15 Evolution of shock speed with different particle activation energy (E in KJ/mol). The particle loading is 400 g/m^3 and particle diameter is 2 μm.

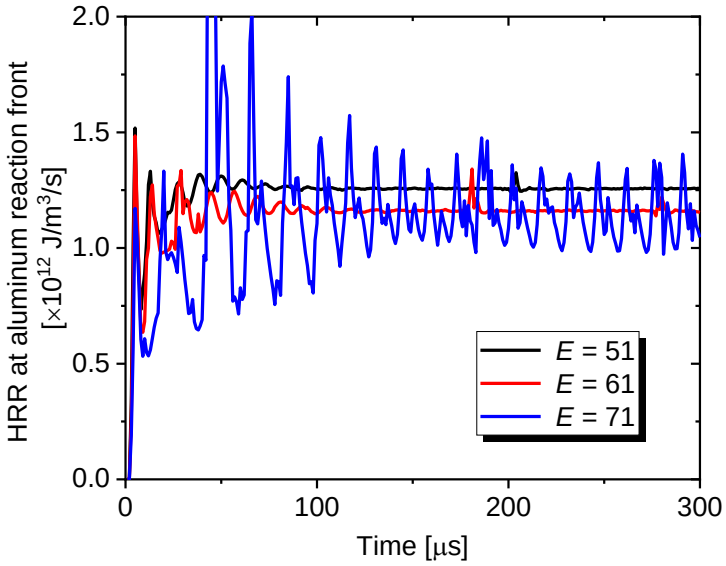

Fig. 16 Aluminum heat release rate at the reaction front for different particle activation energies shown in Fig. 15 (E in KJ/mol).

Figure 15 illustrates the evolution of shock speed for different activation energies (51-91 kJ/mol). For cases with successful initiation, the final average detonation speeds remain similar (~1,975 m/s). However, the results clearly demonstrate a progressive shift in detonation behavior with increasing activation energy: stable propagation at lower activation energies (< 66 kJ/mol), pulsating propagation at intermediate values (~71 kJ/mol), and complete extinction at higher energies (> 81 kJ/mol). Based on Eq. (6), at the same particle temperature, an increase in activation energy effectively reduces the surface reaction rate constant k_s, thereby decreasing the overall heat release. As illustrated in Fig. 16,

this reduction in average heat release slows the progression of surface reactions, thereby limiting the energy available to sustain the detonation front. Consequently, under the same particle mass loading, the system becomes more susceptible to unstable propagation due to insufficient local energy release. The distributions of k_s, k_d, and their ratio (k_s/k_d) for successful initiation cases are presented in Section E of the supplementary material. These results demonstrate that higher activation energy enhances the dominance of surface-kinetic reactions within the particle induction zone. This finding aligns with Zhang et al.'s [5] two-dimensional study of Al-air detonation, which demonstrated that increased activation energy enhances detonation instability, as evidenced by greater cell irregularity.

5. Conclusions

The hybrid detonation of hydrogen-oxygen-argon mixtures containing suspended aluminum particles is numerically investigated using a compressible two-phase flow solver based on the Eulerian-Lagrangian approach. This study systematically examines the influence of two key parameters - particle loading and diameter - on detonation propagation. The hybrid detonation exhibits four distinct regimes based on shock speed characteristics. Regime I features steady propagation with rapidly increasing detonation speed, driven by intensified particle heat release and reduced induction lengths, forming an SFD-like structure. In Regime II, detonation remains steady but slows gradually due to a compression region—formed by interphase momentum and heat transfer before ignition—that weakens the thermal driving effect; this unique quasi-DFD structure may evolve into a typical DFD with larger particles. Regime III is characterized by pulsating propagation, caused by instability in the compression zone: high-pressure waves from the Al reaction front accelerate the shock, while downstream contact discontinuities induce deceleration. Finally, in Regime IV, excessive particle loading leads to decoupling between the shock and reaction fronts, resulting in detonation failure.

Regarding the characteristics of particle combustion, in Regimes I and II, where particle loading is relatively low, both diffusion-controlled and surface-kinetic reactions coexist, with the former being dominant. In Regime III, as the loading increases, surface-kinetic reactions play an increasing role in

aluminum combustion, primarily due to the reduced particle surface temperature within the induction zone. Additional simulations reveal that higher particle activation energies further facilitate the transition from stable to unstable detonation modes.

It is worth noting that further refinement of the hybrid model is required, particularly in representing aluminum–steam surface reactions under extreme conditions. Nevertheless, the present findings enhance our understanding of hybrid detonation dynamics and offer valuable insights for the optimization and control of such systems in practical applications. Future work should explore the effects of polydisperse particles, non-uniform initial distributions, and transverse wave phenomena to more accurately capture real detonation environments.

Declaration of Competing Interest

The authors declare that they have no known competing financial interests or personal relationships that could have appeared to influence the work reported in this paper.

Acknowledgement

This work was supported by National Natural Science Foundation of China (No. 52425604). The computations in this study were performed on the Sugon high-performance supercomputer. P.Z. acknowledges the support from the NUSRI-CQ Research Scholarship.

References

[1] H. Watanabe, A. Matsuo, A. Chinnayya, K. Matsuoka, A. Kawasaki, J. Kasahara, Numerical analysis of the mean structure of gaseous detonation with dilute water spray, J. Fluid Mech. 887 (2020) A4.
[2] M.V. Papalexandris, Numerical simulation of detonations in mixtures of gases and solid particles, J. Fluid Mech. 507 (2004) 95-142.
[3] B. Veyssiere, Detonations in Gas-Particle Mixtures, J. Propul. Power 22 (2006) 1269-1288.
[4] A. Tahsini, Detonation wave attenuation in dust-free and dusty air, J. Loss Prev. Process Ind. 39 (2016) 24-29.
[5] F. Zhang, K. Gerrard, R.C. Ripley, Reaction Mechanism of Aluminum-Particle-Air Detonation, J. Propul. Power 25 (2009) 845-858.
[6] J. Zhang, S. Li, Q. Meng, S. Li, H. Zhang, Detonative wavelets in quasi-detonations with fine coal char particles, Combust. Flame 275 (2025) 114101.

[7] J. Shi, P. Zhang, Y. Xu, W. Ren, H. Zhang, Effects of dilute coal char particle suspensions on propagating methane detonation wave, Combust. Flame 249 (2023) 112618.
[8] D.R. Lide, CRC handbook of chemistry and physics, 96th ed., CRC press(2015).
[9] B. Veyssiere, Double-front detonations in gas-solid particles mixtures, Dynamics of Shock Waves, Explosions, and Detonations, Prog. Astronaut. Aeronaut. 94 (1984) 264-276.
[10] W. Wu, Y. Wang, K. Wu, Z. Ma, W. Han, J. Wang, G. Wang, M. Zhang, Experimental evaluation of aluminum powder fuel in a hydrogen/oxygen detonation tube, Int. J. Hydrogen Energy 48 (2023) 24089-24100.
[11] B. Veyssiere, B. Khasainov, A model for steady, plane, double-front detonations (DFD) in gaseous explosive mixtures with aluminum particles in suspension, Combust. Flame 85 (1991) 241-253.
[12] Q. Zhou, J. Huang, W. Han, C. Wang, Initiation and Propagation of One-Dimensional Detonations in Aluminum-Particle/C2H2/Air system, Phys. Fluids 34 (2022) 102408.
[13] H. Teng, Z. Jiang, Numerical simulation of one-dimensional aluminum particle–air detonation with realistic heat capacities, Combust. Flame 160 (2013) 463-472.
[14] B. Veyssiere, B. Khasainov, Structure and multiplicity of detonation regimes in heterogeneous hybrid mixtures, Shock Waves 4 (1995) 171-186.
[15] X. Yu, X. Yan, J. Yu, W. Gao, Effects of aluminum particle size distributions on the explosion behaviors of hydrogen/aluminum dust hybrid mixtures, Powder Technol. 405 (2022) 117548.
[16] T.A. Khmel, S.A. Lavruk, Simulation of Cellular Detonation Flow in a Hydrogen–Oxygen–Argon Mixture with Aluminum Particles, Combust. Explos. Shock Waves 60 (2024) 374-385.
[17] A.V. Fedorov, T.A. Khmel', Structure and initiation of plane detonation waves in a bidisperse gas suspension of aluminum particles, Combust. Explos. Shock Waves 44 (2008) 163-171.
[18] J. He, B. Meng, B. Tian, H. Li, J. Li, Numerical study of two-phase detonation in dilute aluminum particle-air mixtures using Eulerian-Lagrangian approach, Combust. Flame 275 (2025) 114110.
[19] M. Zhao, Z. Ren, H. Zhang, Pulsating detonative combustion in n-heptane/air mixtures under off-stoichiometric conditions, Combust. Flame 226 (2021) 285-301.
[20] Y. Daimon, A. Matsuo, Detailed features of one-dimensional detonations, Phys. Fluids 15 (2003) 112-122.
[21] W. Han, C. Wang, C.K. Law, Pulsation in one-dimensional H2–O2 detonation with detailed reaction mechanism, Combust. Flame 200 (2019) 242-261.
[22] H. Ng, A. Higgins, C. Kiyanda, M. Radulescu, J. Lee, K. Bates, N. Nikiforakis, Nonlinear dynamics and chaos analysis of one-dimensional pulsating detonations, Combust. Theory Model. 9 (2005) 159-170.
[23] H.D. Ng, M.I. Radulescu, A.J. Higgins, N. Nikiforakis, J.H.S. Lee, Numerical investigation of the instability for one-dimensional Chapman–Jouguet detonations with chain-branching kinetics, Combust. Theory Model. 9 (2005) 385-401.
[24] Y. Xu, H. Zhang, Pulsating propagation and extinction of hydrogen detonations in ultrafine water sprays, Combust. Flame 241 (2022) 112086.
[25] S. Yungster, K. Radhakrishnan, Pulsating one-dimensional detonations in hydrogen–air mixtures, Combust. Theory Model. 8 (2004) 745-762.
[26] Y. Daimon, A. Matsuo, Unsteady features on one-dimensional hydrogen-air detonations, Phys. Fluids 19 (2007) 549.
[27] Y.-C. Cheng, J.-Q. Zhao, S.-W. Liao, C.-M. Shu, Explosion mechanism of aluminum powder mixed with low-concentration hydrogen, Int. J. Hydrogen Energy 47 (2022) 27293-27302.
[28] U. Uphoff, D. Hänel, P. Roth, Numerical modelling of detonation structure in two-phase flows, Shock Waves 6 (1996) 17-20.
[29] M.P. Burke, M. Chaos, Y. Ju, F.L. Dryer, S.J. Klippenstein, Comprehensive H2/O2 kinetic model for high-pressure combustion, Int. J. Chem. Kinet. 44 (2012) 444-474.
[30] Z.J. Zhang, C.Y. Wen, Y.F. Liu, D.L. Zhang, Z.L. Jiang, Effects of Different Particle Size Distributions on Aluminum Particle–Air Detonation, AIAA J. 58 (2020) 3115-3128.

[31] T. Khmel, S. Lavruk, Detonation flows in aluminium particle gas suspensions, inhomogeneous in concentrations, J. Loss Prev. Process Ind. 72 (2021) 104522.
[32] P. Zhang, H. Zhang, Y.F. Zhang, S. Li, Q. Meng, Modeling particle collisions in moderately dense curtain impacted by an incident shock wave, Phys. Fluids 35 (2023) 023327.
[33] P. Zhang, H. Zhang, Instabilities of a circular moderately dense particle cloud impacted by an incident shock, Int. J. Multiphase Flow 174 (2024) 104787.
[34] P. Zhang, C. Cao, H. Zhang, Micron-sized aluminum particle combustion under elevated gas condition: equivalence ratio effect, Appl. Energy Combust. Sci. 19 (2024) 100283.
[35] P. Zhang, Y.F. Zhang, Z. Chen, H. Zhang, Combustion of Micro Aluminum Particle Suspension Behind an Incident Shock Wave, Available at SSRN 5104519. doi: http://dx.doi.org/10.2139/ssrn.5104519.
[36] J. Capecelatro, J.L. Wagner, Gas–particle dynamics in high-speed flows, Annu. Rev. Fluid Mech. 56 (2024) 379-403.
[37] E. Loth, J. Tyler Daspit, M. Jeong, T. Nagata, T. Nonomura, Supersonic and Hypersonic Drag Coefficients for a Sphere, AIAA J. 12 (2021) 3261-3274.
[38] D.S. Sundaram, P. Puri, V. Yang, A general theory of ignition and combustion of nano- and micron-sized aluminum particles, Combust. Flame 169 (2016) 94-109.
[39] D.-H. Han, H.-G. Sung, A numerical study on heterogeneous aluminum dust combustion including particle surface and gas-phase reaction, Combust. Flame 206 (2019) 112-122.
[40] Z. Zhang, C. Wen, Y. Liu, D. Zhang, Z. Jiang, Application of CE/SE method to gas-particle two-phase detonations under an Eulerian-Lagrangian framework, J. Comput. Phys. 394 (2019) 18-40.
[41] M.W. Beckstead, A Summary of Aluminum Combustion, Report No. RTO-EN-023, The Research and Technology Organisation of NATO, (2002).
[42] D.R. Dyson, H. Patel, R.I. Yuraszeck, A.J. Puerta-Alvarado, S. Vasu, R.W. Houim. Aluminum Powder Oxidation in a Hydrogen-Oxygen Post-Detonation Environment. AIAA SCITECH 2025 Forum; (2025), p. 2534.
[43] K. Benkiewicz, A.K. Hayashi, Parametric studies of an aluminum combustion model for simulations of detonation waves, AIAA J. 44 (2006) 608-619.
[44] Y. Liang, M. Beckstead. Numerical simulation of quasi-steady, single aluminum particle combustion in air. 36th AIAA Aerospace Sciences Meeting and Exhibit; (1998), p. 254.
[45] A. Briand, B. Veyssiere, B.A. Khasainov, Modelling of detonation cellular structure in aluminium suspensions, Shock Waves 20 (2010) 521-529.
[46] Y. Xu, P. Zhang, Q. Meng, S. Li, H. Zhang, Transmission of hydrogen detonation across a curtain of dilute inert particles, Combust. Flame 254 (2023) 112834.
[47] A. Borisov, B. Khasainov, E. Saneev, I. Formin, S. Khomik, B. Veyssiere, On the detonation of aluminum suspensions in air and in oxygen, Dynamic structure of detonation in gaseous and dispersed media (1991) 215-253.
[48] F. Zhang, Detonation in reactive solid particle-gas flow, J. Propul. Power 22 (2006) 1289-1309.
[49] F. Zhang, S.B. Murray, K.B. Gerrard, Aluminum Particles–air Detonation at Elevated Pressures, Shock Waves 15 (2006) 313-324.
[50] B. Veyssiere, W. Ingignoli, Existence of the detonation cellular structure in two-phase hybrid mixtures, Shock Waves 12 (2003) 291-299.
[51] J.D. Anderson, Modern compressible flow with historical perspective, 2nd ed., McGraw Hill, New York, (1990).
[52] A. Matsuo, T. Fujiwara, Numerical investigation of oscillatory instability in shock-induced combustion around a blunt body, AIAA J. 31 (1993) 1835-1841.
[53] Y. Kamiyama, A. Matsuo, Flow features of shock-induced combustion around cylindrical projectiles, Proc. Combust. Inst. 28 (2000) 671-677.
[54] A. Matsuo, K. Fujii, Computational study of large-disturbance oscillations in unsteady supersonic combustion around projectiles, AIAA J. 33 (1995) 1828-1835.
[55] C. Leung, M.I. Radulescu, G.J. Sharpe, Characteristics analysis of the one-dimensional pulsating dynamics of chain-branching detonations, Phys. Fluids 22 (2010) 539.

[56] A. Matsuo, K. Fujii, T. Fujiwara, Flow features of shock-induced combustion around projectile traveling at hypervelocities, AIAA J. 33 (1995) 1056-1063.